STANDARD ARTICLE

Journal of Veterinary Internal Medicine ACVIM

Open Access

American College of Veterinary Internal Medicine

Persistent fontanelles in Chihuahuas. Part I. Distribution and clinical relevance

Anna-Mariam Kiviranta[1] | Clare Rusbridge[2,3] | Anu K. Lappalainen[1] |
Jouni J. T. Junnila[4] | Tarja S. Jokinen[1]

[1]Department of Equine and Small Animal Medicine, Faculty of Veterinary Medicine, University of Helsinki, Helsinki, Finland

[2]School of Veterinary Medicine, Faculty of Health and Medical Sciences, University of Surrey, Guildford, United Kingdom

[3]Fitzpatrick Referrals, Godalming, United Kingdom

[4]4Pharma Ltd, Helsinki, Finland

Correspondence
Anna-Mariam Kiviranta, Department of Equine and Small Animal Medicine, University of Helsinki, 00014 Helsinki, Finland.
Email: anna-mariam.kiviranta@helsinki.fi

Abstract

Background: The Chihuahua dog breed is known for frequent occurrence of a bregmatic fontanelle on the dorsal skull. A common conception is that this skull defect is a clinically irrelevant finding. No studies, however, describe its prevalence or whether it is accompanied by other persistent fontanelles (PFs). Although Chihuahuas are predisposed to Chiari-like malformation (CM) and syringomyelia (SM), it is unknown whether PFs occur more commonly in dogs with clinical signs that are caused by CM or SM.

Hypothesis/Objectives: To describe the number and location of PFs at cranial sutures (CSs) and to compare the occurrence of these PFs in dogs with and without CM/SM-related clinical signs. We hypothesized that PFs also occur commonly at lateral and caudal cranial surfaces, affect a higher number of CSs, and are larger in dogs with CM/SM-related clinical signs.

Animals: Fifty client-owned Chihuahuas with or without CM/SM-related clinical signs.

Results: Of the 50 dogs evaluated, 46 (92%) had either 1 or several PFs. The mean ± SD number of PFs was 2.8 ± 3.0 (range, 0-13). A total of 138 PFs occupied 118 CSs with 57 (48%) located dorsally, 44 (37%) caudally, and 17 (14%) laterally. The number of CSs affected by PFs was significantly higher ($P \leq .001$) and total PF area was significantly larger ($P = .003$) in dogs with CM/SM-related clinical signs.

Conclusions and Clinical Importance: Persistent fontanelles are very common in this group of Chihuahuas and appear at dorsal, lateral, and caudal cranial surfaces. They are more numerous and larger in Chihuahuas with CM/SM-related clinical signs.

KEYWORDS
Chiari-like malformation, Chihuahua, craniocervical junction, fontanelle, ossification, syringomyelia

---

- - - - - - - - - -

1 | INTRODUCTION

The Chihuahua is a dog breed known for its very small size, round head, and frequent occurrence of a persistent, bregmatic fontanelle (BF) on the dorsal skull, between the paired frontal and parietal bones. A common assumption is that in small breed dogs, and especially in Chihuahuas, the BF (molera) is a clinically irrelevant finding.[1] No studies, however, describe the prevalence of this malformation, state whether it is accompanied by persistent fontanelles (PFs) at other locations on the skull, or evaluate its clinical relevance.

In Chihuahuas, abnormalities related to craniocervical development causing craniocervical junction (CCJ) overcrowding including Chiari-like malformation (CM), medullary elevation, and dorsal spinal cord compression at C1-2 are common. Furthermore, this breed commonly has syringomyelia (SM). In Chihuahuas, both SM and CCJ junction overcrowding are associated with CM/SM-related clinical signs such as pain-related behavior or gait abnormalities.[2] No studies, however, have evaluated whether dogs with these CM/SM-related clinical signs are more predisposed to PFs.

Fontanelles are fibrous, membrane-covered gaps that lie between the cranial bones at the intersection of the cranial sutures (CSs). In dogs, the literature describes the BF and the fontanelle between the interparietal and supraoccipital bones, here called the occipital fontanelle. Children, however, are born with 6 fontanelles: 2 along the midline, called the anterior and the posterior fontanelles, as well as 2 on each side of the skull: the left and right sphenoid, and the left and right mastoid fontanelles.[4] The canine BF is equivalent to the human anterior fontanelle and the canine occipital fontanelle resembles the posterior fontanelle in children. Fontanelles equivalent to human sphenoid or mastoid fontanelles have not been described in dogs.

The CSs are the junctions between the cranial bones and form the intersections in which the fontanelles are located. They serve as the major sites of bone expansion during postnatal cranial growth of the cranial vault that accommodates the enlarging brain. This expansion occurs in response to signals from the expanding neurocranium and dura mater.[5,6] At maturation, further growth of the cranium is disabled and the cranial fontanelles and sutures close. In dogs, BF closure is assumed to occur at birth or within a month afterward, and the occipital fontanelle closes at approximately 45 days of gestation.[3,7]

The 2 aims of our study were to describe, in Chihuahuas, the presence, number, and location of PFs, and to compare the occurrence of PFs in dogs with and without CM/SM-related clinical signs. Our hypotheses were that PFs are common and occur at other locations in addition to the BF. Furthermore, we hypothesized that, in Chihuahuas, PFs are more numerous and larger in dogs with CM/SM-related clinical signs.

2 | MATERIALS AND METHODS

2.1 | Case selection and assessment of clinical signs

Our data included 50 Chihuahuas with or without CM/SM-related clinical signs. The dogs underwent both magnetic resonance imaging (MRI) and computed tomography (CT). These dogs all were recruited from the caseload of the Veterinary Teaching Hospital of the University of Helsinki between 2012 and 2015. They were members of the same cohort (one comprising 53 Chihuahuas) participating in another, concurrent study published earlier.[2] Imaging of the clinically affected dogs was a diagnostic procedure, and the nonclinically affected dogs were imaged for breeding selection to detect CM, SM, and CCJ abnormalities (including atlanto-occipital overlapping, medullary elevation, and dorsal spinal cord compression at C1-2 associated with atlantoaxial bands). We used previously described methods to image and define SM and CCJ abnormalities.[2] The study was approved by the Finnish National Animal Experiment Board, participation was voluntary, and each dog owner provided written consent.

To be included in the study, nonaffected dogs had to be at least 3 years old and have no signs of illness (confirmed using a questionnaire and an owner interview during the clinic visit). No age limit was set for those dogs with CM/SM-related clinical signs. We excluded all dogs with severe orthopedic disease because such disease could cause gait abnormalities similar to those observed in SM-affected dogs (Figure 1). Furthermore, all dogs with prior history of or a current finding of another central nervous system disease on MRI (other than CM, SM, ventriculomegaly, or CCJ overcrowding) were excluded, because these conditions could affect cerebrospinal fluid flow.

To categorize the dogs as clinically affected or unaffected by CM/SM required a questionnaire similar to that used in an earlier study[2] inquiring as to any persistent scratching episodes (ears, cervical region, shoulders, or cranial thoracic spine) with or without skin contact, facial rubbing, spinal pain, vocalization, and gait abnormalities such as incoordination or weakness. Dogs with any of these clinical signs, we assigned to the cohort with CM/SM-related clinical signs. Because 7 of the clinically affected dogs had concurrent health problems observed either during history taking or clinical examination, we excluded these from assessment of CM/SM-related clinical signs, but included them in image analysis of the PFs (Figure 1).

2.2 | Diagnostic imaging procedures

All dogs underwent CT and MRI under general anesthesia. As a diagnostic procedure, and to exclude other diseases causing clinical signs similar to those of CCJ overcrowding or SM, we obtained MR images of the head and cervical spine using a 0.2 Tesla MR scanner (Esaote S. p.A, Genova, Italy; Table 1). We positioned each dog in sternal recumbency with the base of the skull aligned perpendicular to the ventral vertebral canal at the first 2 cervical vertebrae.

To obtain head and cervical spine (to the level of the caudal C3 vertebra) CT images, we used a helical dual-slice CT scanner (Somatom Emotion Duo, Siemens AG, Forcheim, Germany), with a bone algorithm and a slice thickness of 1.0 mm (feed/rotation 2 mm, reconstruction increment 0.5 mm, 110 kV). Each dog was positioned so that the base of the skull was aligned perpendicular to the ventral vertebral canal in the cranial cervical spine.
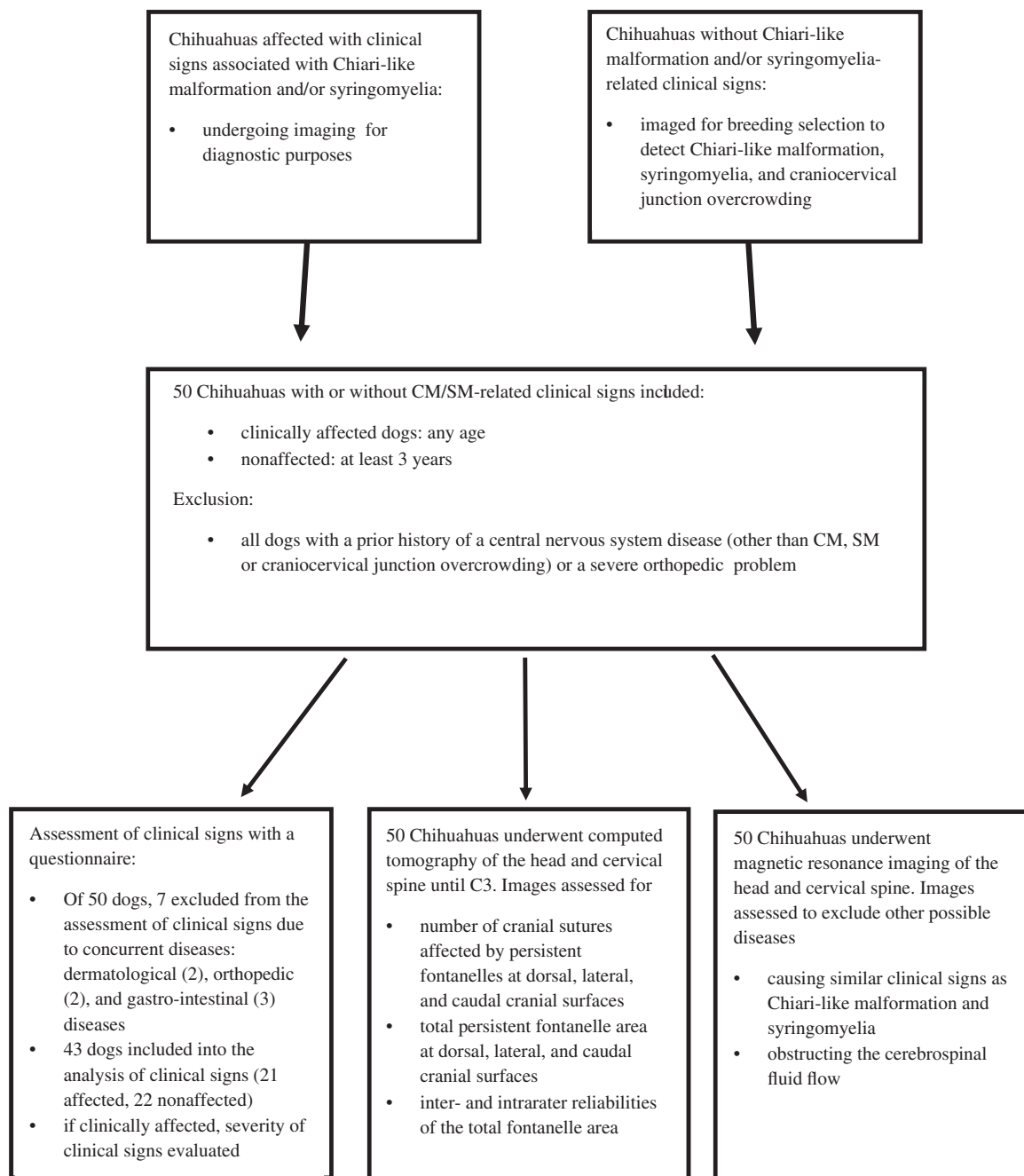
Chihuahuas affected with clinical signs associated with Chiari-like malformation and/or syringomyelia:

- undergoing imaging for diagnostic purposes

Chihuahuas without Chiari-like malformation and/or syringomyelia-related clinical signs:

- imaged for breeding selection to detect Chiari-like malformation, syringomyelia, and craniocervical junction overcrowding

50 Chihuahuas with or without CM/SM-related clinical signs included:

- clinically affected dogs: any age
- nonaffected: at least 3 years

Exclusion:

- all dogs with a prior history of a central nervous system disease (other than CM, SM or craniocervical junction overcrowding) or a severe orthopedic problem

Assessment of clinical signs with a questionnaire:

- Of 50 dogs, 7 excluded from the assessment of clinical signs due to concurrent diseases: dermatological (2), orthopedic (2), and gastro-intestinal (3) diseases
- 43 dogs included into the analysis of clinical signs (21 affected, 22 nonaffected)
- if clinically affected, severity of clinical signs evaluated

50 Chihuahuas underwent computed tomography of the head and cervical spine until C3. Images assessed for

- number of cranial sutures affected by persistent fontanelles at dorsal, lateral, and caudal cranial surfaces
- total persistent fontanelle area at dorsal, lateral, and caudal cranial surfaces
- inter- and intrarater reliabilities of the total fontanelle area

50 Chihuahuas underwent magnetic resonance imaging of the head and cervical spine. Images assessed to exclude other possible diseases

- causing similar clinical signs as Chiari-like malformation and syringomyelia
- obstructing the cerebrospinal fluid flow

FIGURE 1   A flowchart describing the procedures of the study

2.3 | Image analysis

Two board-certified neurologists (C. Rusbridge, T.S. Jokinen), blinded to the presence or absence of CM/SM-related clinical signs, independently evaluated the MR images for CM, SM, or other abnormalities that could cause similar clinical signs or affect cerebrospinal fluid flow. OsiriX Medical Imaging Software (Pixmeo SARL, Bernex, Switzerland) was used for analysis of the CT images of all included dogs for presence, number, location, and area of the PFs at dorsal, lateral, and caudal CSs. Two board-certified neurologists (A.-M. Kiviranta and T.S. Jokinen) independently evaluated the

anonymized CT images and were hence unaware of any dogs' clinical status.

2.3.1 | Definition of PFs

A PF was defined as full-thickness loss of bone at a CS. Its presence was assessed at the CSs, that is at junctions between the membrane-derived bones (nasal, lacrimal, frontal, parietal, interparietal, squamous part of the temporal) and between membrane- and cartilage-derived bones (maxillary, palatine, sphenoid, temporal, occipital) that form the

	Dogs without CM/SM-related clinical signs	Dogs with CM/SM-related clinical signs
T1W sagittal	x	x
T1W transverse	x	x
T2W sagittal	x	x
T2W transverse[a]		x

Abbreviations: CM, Chiari-like malformation; SM, syringomyelia; W, weighted.

[a]In dogs without CM/SM-related clinical signs, the cervical spine was imaged until the caudal end of the fourth cervical vertebra. In dogs with CM/SM-related clinical signs, the entire cervical spinal cord was imaged. The slice thickness ranged from 3.5 to 4.5 mm. If syringomyelia was detected, transverse slices were adjusted to the center of it.

dorsal, lateral, and caudal surfaces of the braincase (Table 2, Figures 2A-C). The cranial base, formed of cartilage-derived bones connected with synchondroses, and naturally occurring with multiple foramina, was not evaluated. To avoid including nonfused, normal CSs, the fontanelle area had to be large enough, by subjective assessment, to be measurable using the closed polygon tool of the Osirix Medical Imaging Software. The smallest PFs were approximately 1 mm in diameter.

2.3.2 | Evaluation of PFs and CSs affected

The evaluators first assessed each CS in 3-dimensional skull models using volume-rendering technique images to record the presence and number of all possible PFs (Figures 3A-D). Then, the finding of an area deficient with bone (full-thickness) was confirmed in the multiplanar images (Figure 4A-C).

In addition to identifying the presence of a PF, we located the suture that the PF affected. Because the distinction between some dorsal and lateral bones was difficult because of their small size and irregular shape, we made no attempt to distinguish between the sutures they affected; instead, we classified these sutures as 1 (Table 2, Figure 2A-C). Furthermore, because a PF occasionally was located between the supraoccipital and interparietal bones, but not at a true suture, this location was considered an additional location in the analysis.[3] Additionally, the intersections of the lateral sutures, resembling sphenoid and mastoid fontanelles in children, were classified as additional locations.[8]

If, after the individual assessment, the evaluators disagreed as to the presence or number of PFs, or as to the sutures affected, the evaluators together reassessed the CT images to reach consensus.

2.3.3 | Persistent fontanelle area measurement

After reaching consensus as to the number and location of the PFs, the evaluators independently measured the area of each fontanelle from the anonymized CT images (WL 500 HU, WW of 3500 HU; Figure 4D). Because PF size varied markedly, we consequently elected to measure the area of the PFs. We aimed to compare the extent (area) of these bone-deficient lesions in clinically affected and nonaffected dogs in addition to comparing the number of the affected sutures. Because the PFs were occasionally so large and extended over convex surfaces (eg, on the top of the head at the bregma), it was impossible in multiplanar images to measure the area of the PFs in a single plane. We used maximum-intensity projection-technique images for the area measurement. This technique overcame the problem of bias from exclusion from analysis of large PFs located at convex surfaces. It also overcame the problem of measuring the PF area by repositioning the index lines. We visually selected a slice thickness of 14 to 16 mm, which optimized our ability to measure the convex surfaces without the area to be measured being affected. We tested this approach by assessing CT images of 10 pilot dogs not included in the study.

The fontanelle area measurement was carried out by first positioning 1 of the 2 index lines tangential to the outer skull surface, and in the mid-thickness of the bone surrounding it. Then, the other index line was positioned perpendicular to the previous index line and in the center of the PF (Figure 4A-C). After index line positioning, slice thickness was adjusted, and PF area was measured using a closed polygon tool (Figure 4D).

2.4 | Statistical analysis

2.4.1 | Inter- and intrarater reliability of the total fontanelle area measurement

To evaluate the repeatability of the PF area measurement method, we evaluated the inter- and intrarater repeatability of the total PF areas (a sum of the area of all PFs in each dog). We evaluated the random variation between assessors (inter-rater reliability) in 2 different ways. First, we calculated a repeatability statistic between the assessors from a 1-way analysis of variance model, where the effect of the dog served as the sole fixed effect, and the values were considered as a percentage of perfect agreement. In these models, the within-group variation describes the variation between the assessors.

Second, to determine inter-rater reliability estimate between the 2 assessors, we calculated Krippendorff's alpha with 95% confidence intervals (CIs) to assess consistency between the 2 assessments of the total PF areas.[9] An alpha value of 1 describes perfect agreement, a value of 0.8 describes similar interpretation, and a value of 0.67 is interpreted as the lowest conceivable limit.[10]

Next, we evaluated intrarater reliability. After a few months, the 2 evaluators independently remeasured the PF areas of 25 of 50 randomly selected dogs. Because the method was labor-intensive, the CT images of 25 dogs were re-evaluated. Intrarater reliability assessment was evaluated using 2 different methods. First, we calculated a repeatability statistic similar to that for inter-rater reliability between the 2 repeats (total PF area) by each evaluator. Second, to determine the intrarater reliability estimate between the repeats, we calculated the intraclass correlation coefficient (ICC) with 95% CIs to assess consistency between the repeats. An ICC of <0.5 indicated poor reliability, 0.5 to 0.75 moderate reliability, 0.75 to 0.9 good reliability, and >0.9 indicated excellent reliability.[11]

TABLE 2 Distribution and number of persistent fontanelles in Chihuahuas of this study

Location	Bone	Connecting bone	Suture/intersection	Human /canine fontanelle equivalent	Number of dogs	Number of sutures	% of all sutures	Number of fontanelles	% of fontanelles
Dorsal sutures	Frontal	Nasal, maxillar, lacrimal	Frontonasal, frontomaxillar, frontolacrimal	NA	49	2	1.7	2	1.4
		Frontal	Interfrontal	NA	49	4	3.4	4	2.9
		Parietal	Frontoparietal/at the intersection of the interfrontal, frontoparietal, and sagittal sutures	Bregmatic (at the intersection)	49	39	33.1	54/46	38.8/33.3
	Parietal	Parietal	Sagittal	NA	49	0	0	0	0
		Left interparietal	Left parietointerparietal	NA	49	6	5.1	6	4.3
		Right interparietal	Right parietointerparietal	NA	49	6	5.1	6	4.3
Lateral sutures	Frontal	Palatinal, sphenoid	Left frontopalatine, sphenofrontal	NA	50	1	0.8	1	0.7
			Right frontopalatine, sphenofrontal	NA	50	1	0.8	1	0.7
		Sphenoid, parietal	Left intersection	Left sphenoid	50	3	2.5	3	2.2
			Right intersection	Right sphenoid	50	4	3.4	4	2.9
	Parietal	Sphenoid, temporal	Left sphenoparietal, squamous	NA	50	3	2.5	3	2.2
			Right sphenoparietal, squamous	NA	50	5	4.2	5	3.6
Caudal sutures	Occipital	Parietal	Left occipitoparietal	NA	50	4	3.4	4	2.9
			Right occipitoparietal	NA	50	7	5.9	9	6.5
		Parietal, temporal	Left intersection	Left mastoid	50	12	10.2	13	9.4
			Right intersection	Right mastoid	50	14	11.9	15	10.9
		Temporal	Left occipitosquamous	NA	50	1	0.8	1	0.7
			Right occipitosquamous	NA	50	2	1.7	2	1.4
		Interparietal	Not a true suture	Posterior	50	4	3.4	5	3.6

Note: The sutures are grouped by dorsal, lateral, and caudal surfaces, and the bones that the sutures are connecting are nominated. In case the sutural intersections form a fontanelle, the veterinary or a human equivalent term is given.
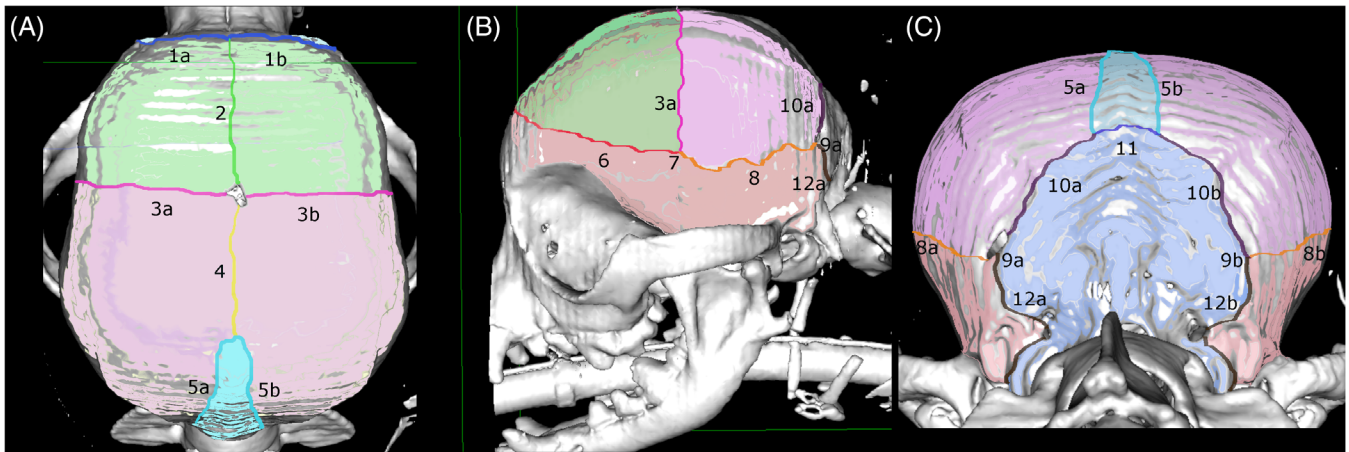
Abbreviation: NA, not applicable.

FIGURE 2 A-C, Dorsal, lateral, and caudal volume-rendering technique computed tomography images (window level 500, window width 3500) of a Chihuahua skull showing the cranial sutures evaluated in this study. Numbers 1 to 5 mark dorsal cranial sutures, 6 to 8 lateral cranial sutures, and 9 to 12 caudal cranial sutures evaluated: 1a (left), 1b (right): frontonasal, frontomaxillar, and frontolacrimal sutures; 2: interfrontal suture; 3a-b: frontoparietal suture, 4: sagittal suture, 5a-b: parietointerparietal suture, 6: left frontopalatine and sphenofrontal sutures, 7: intersection of left frontoparietal, sphenofrontal, and sphenoparietal sutures (resembling sphenoid fontanelle in children); 8: left sphenoparietal and squamous sutures; 9a-b: intersection of squamous, occipitoparietal, and occipitosquamous sutures (resembling mastoid fontanelle in children); 10a-b: occipitoparietal suture, 11: junction between occipital and interparietal bones (not a true suture); 12a-b: occipitosquamous suture

FIGURE 3 A-D, Volume-rendering technique computed tomography image of Chihuahua skulls in dorsal (A, B), right lateral (C), and caudal (D) views showing (A): single, sharply demarcated, persistent bregmatic fontanelle at the intersection of paired frontal and parietal cranial bones (the frontoparietal suture). B, Multiple bregmatic fontanelles. C, Single, sharply demarcated persistent fontanelle at the intersection of frontal, sphenoidal, and parietal bones, resembling location of the right sphenoidal fontanelle in children. D, Multiple persistent fontanelles on a caudal cranial surface: persistent fontanelles marked with a red star were confirmed, in multiplanar images, as penetrating through the bone. Other lesions appearing as persistent fontanelles (no red star) are areas of thin bone
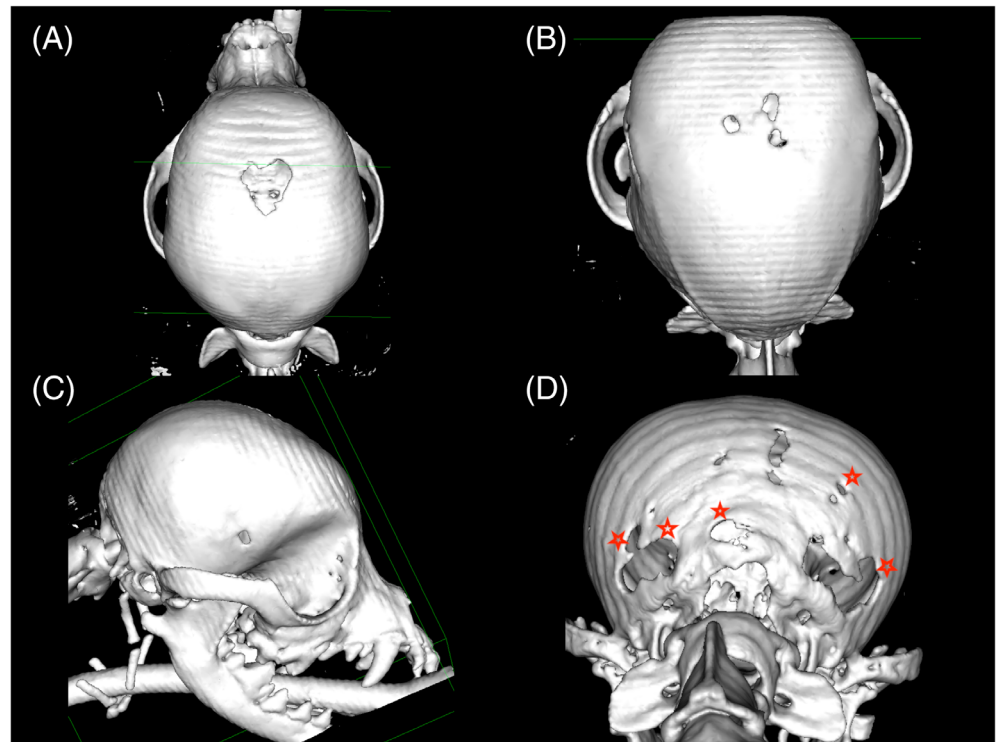
2.4.2 | Persistent fontanelles in dogs with and without CM/SM-related clinical signs

When comparing the dogs with and without CM/SM-related clinical signs, for each dog we used both the total number of CSs affected by PFs and total PF area. For this comparison, we used the number of affected CSs instead of the number of PFs, because occasionally several PFs occupied a single suture. For statistical analysis of the number of affected CSs, we used univariate Poisson regression. The total number of CSs affected by PFs served as the response and CM/SM-related clinical signs served as explanatory factor.
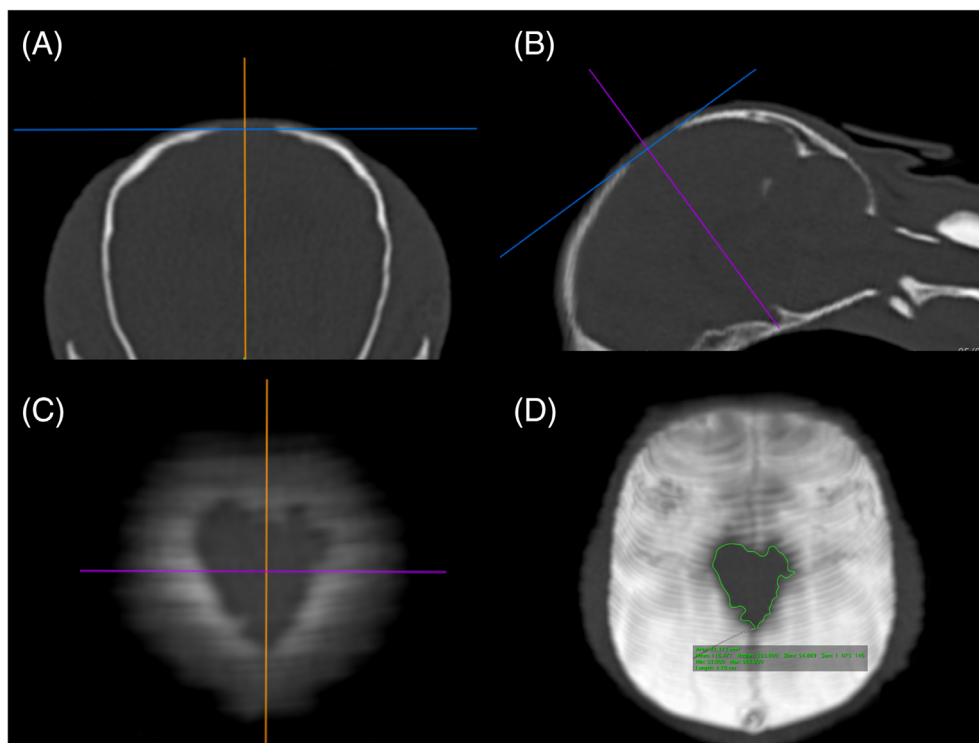
FIGURE 4 A-D, Positioning of index lines and persistent fontanelle area measurement. Transverse (A), sagittal (B), dorsal (C) multiplanar, and maximum-intensity projection (D) computed tomography images (window level 500, window width 3500, slice thickness 1 mm) showing position of index lines positioned with the first index line tangential to the outer skull surface and in the mid-thickness of its surrounding bone (blue index line). Second index line positioned perpendicular to previous index line and in the center of the persistent fontanelle [orange index line in (A), purple index line in (B)]. In dorsal view (C), intersection of index lines positioned at the center of the persistent fontanelle. Area of the bregmatic fontanelle, 82.4 mm^2, measured by OsiriX Medical Imaging Software's closed polygon tool (D)

In addition to comparing the number of CSs affected by PFs, we compared the total PF area of the dogs with and without CM/SM-related clinical signs. The mean of the 2 measurements (from the 2 evaluators) served for the analysis. In the statistical analysis, the total PF area was first log-transformed to satisfy the normality assumptions of the statistical modeling. The normality of the model residuals was investigated using Shapiro-Wilks tests and Normal QQ-plots. Because there were some zero observations (ie, dogs without PFs), the transformation was conducted logarithmically (total sum of PF areas +1). The analysis utilized a 1-way analysis of variance model. The log-transformed total PF area served as the response, and the CM/SM-related clinical signs served as explanatory factors. P values of <.05 were considered statistically significant; all P values are 2-sided and not adjusted for multiple testing. All statistical analyses were conducted using SAS System for Windows, version 9.4 (SAS Institute, Inc, Cary, North Carolina).

3 | RESULTS

The study group consisted of 50 Chihuahuas (Table 3). The mean ± SD age of the 50 dogs was 58 ± 28 months (range, 7-139 months), and their mean ± SD weight was 2.8 ± 0.6 kg (range, 1.4-4.3 kg).

3.1 | Presence, number, and location of PFs

Of the 50 dogs evaluated, 46 (92%) had either 1 or several PFs, and 4 dogs (8%) lacked any PFs (Table 4). The mean ± SD number of PFs per dog was 2.8 ± 3.0 (range, 0-13), and the mean ± SD number of CSs affected by a PF was 2.4 ± 2.3 (range, 0-10; Figures 5 and 6). Because 1 dog had missing CT images of the rostral skull, the cohort for evaluation of distribution of PFs and affected sutures consisted of 49 dogs (Table 2). In these 49 dogs, 138 PFs were identified, with 72 (52%) appearing dorsally, 49 (36%) caudally, and 17 (12%) laterally (7 on the left side, 10 on the right side). Furthermore, the 138 PFs occupied a total of 118 CSs with 57 (48%) located dorsally, 44 (37%) caudally, and 17 (14%) laterally (7 on the left side, 10 on the right side).

The frontoparietal suture was most commonly affected in 39 (78%) of 50 dogs and comprised 54 (39%) of the 138 PFs. Of 54 PFs at the frontoparietal suture, 46 (85%) emerged at the intersection of the interfrontal, frontoparietal, and sagittal sutures, which is the location of the BF. Furthermore, of the 138 PFs, 86 (62%) occurred at locations similar to those of the fontanelles in children (the anterior, posterior, sphenoid, or mastoid fontanelles), leaving 44 (38%) of the 138 PFs occurring at other locations (Table 2).

TABLE 3 Signalment and diagnostic imaging findings in all 50 Chihuahuas

Signalment	Number of dogs (%)
Smooth-haired Chihuahuas	26 (52%)
Long-haired Chihuahuas	23 (46%)
Chihuahua-mix	1 (2%)
Female	27 (54%)
Male	23 (46%)[a]
Diagnostic imaging findings	
Chiari-like malformation	50 (100%)
Syringomyelia	20 (40%) (syrinx width 2-8 mm)
AOO	35 (70%)
Mean ± SD medullary kinking index	22% ± 8% (range, 6%-43%)
Mean ± SD dorsal spinal cord compression index	25% ± 7% (range, 9%-38%)

Abbreviation: AOO, atlanto-occipital overlapping.
[a]Including one castrated male.

Evaluation of the 46 dogs having at least 1 PF showed that 7 (15%) had no PF at a location typical of a BF (Table 4). Of those dogs, each dog had 1 to 7 affected sutures on dorsal, lateral, or caudal cranial surfaces.

3.2 | Inter- and intrarater reliability of PF area measurement in CT images

The inter-rater repeatability of the total fontanelle area measurements between the assessors was 99.8%. When assessing consistency between the 2 assessments, Krippendorff's alpha for the total fontanelle area was 0.999 (95% CI, 0.997-1.000; Table 5).

The intrarater repeatability of the total fontanelle area measurements was 99.6% for 1 and 99.8% for the other assessor. Furthermore, the ICC for reliability within assessor of the total fontanelle area ranged from 0.997 to 0.999 (95% CI, 0.994-0.999; Table 6).

TABLE 4 Signalment and imaging findings of the 4 dogs lacking any persistent fontanelles and 7 dogs lacking a bregmatic fontanelle

Variable	4 dogs lacking any persistent fontanelles	7 dogs lacking a bregmatic fontanelle
Mean age (range)	56 months (range, 23-89 months)	58 months (range, 12-91 months)
Mean weight	3.2 kg (range, 2.7-4.3 kg)	3.0 kg (range, 1.8-3.9 kg)
Number of dogs with SM (%)	1/4 (25%) Maximum syrinx width 3.5 mm	3/7 (43%) Range of maximum syrinx width 2-2.7 mm
Dogs with clinical signs related to CM/SM	1/3[a] (33%)	3/6[a] (50%)

Abbreviations: CM, Chiari-like malformation; SM, syringomyelia.
[a]One dog excluded from the analysis of clinical signs because of other, concurrent diseases possibly causing similar clinical signs.
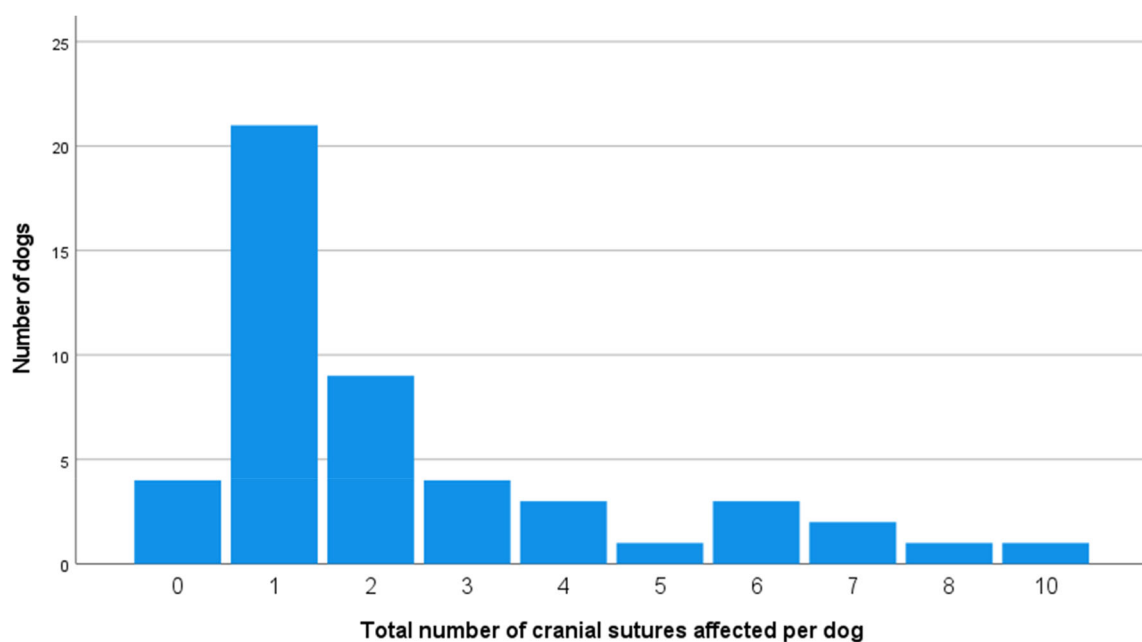
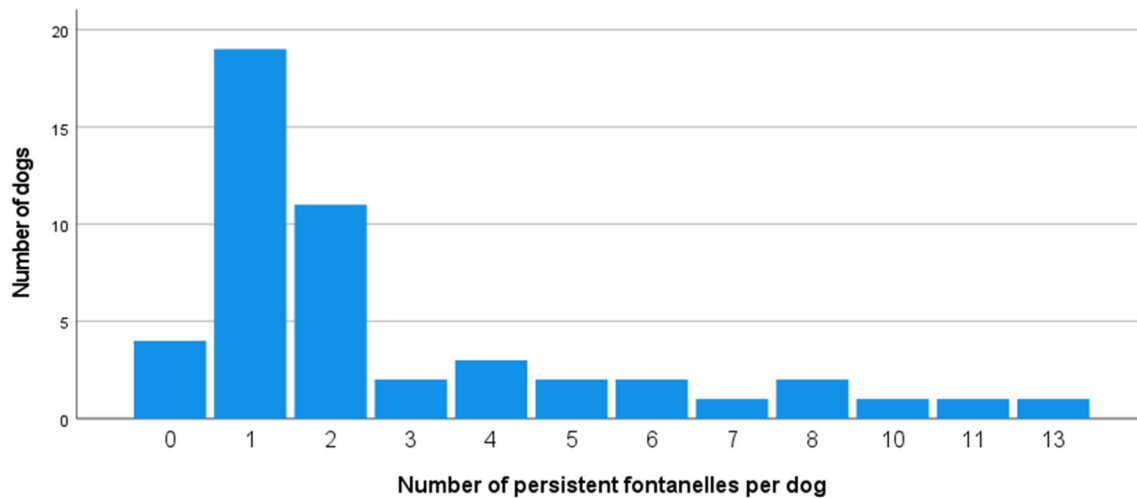**FIGURE 5** Total number of cranial sutures affected per dog

FIGURE 6 Total number of presented fontanelles per dog

TABLE 5 Inter-rater reliability: repeatability and Krippendorff's alpha reliability estimates between assessors

Area measured	Assessor 1 (mm^2)	Assessor 2 (mm^2)	Repeatability (%)	Alpha	95% CI	Number of pairs
Total fontanelle area (mean ± SD)	78.4 ± 149.8	77.8 ± 148.8	99.8	0.999	0.997-1.000	50
Dorsal fontanelle area (mean ± SD)	44.8 ± 55.8	44.2 ± 54.3	99.6	0.997	0.995-0.999	50
Left lateral fontanelle area (mean ± SD)	65.2 ± 106.9	67.0 ± 111.5	99.7	0.998	0.995-1.000	6
Right lateral fontanelle area (mean ± SD)	48.9 ± 97.8	46.9 ± 97.2	99.5	0.996	0.989-1.000	9
Caudal fontanelle area (mean ± SD)	17.0 ± 38.1	17.1 ± 37.7	99.6	0.997	0.994-0.999	50

Note: Inter-rater reliability: repeatability and Krippendorff's alpha reliability estimates of total, dorsal, left and right lateral, and caudal fontanelle area measurements between the two assessors.
Abbreviation: CI, confidence interval.

TABLE 6 Intrarater reliability: fontanelle area intraclass correlation coefficient

	Assessor 1		Assessor 2		Combined	
Area measured	ICC	95% CI	ICC	95% CI	ICC	95% CI
Total fontanelle area	0.999	0.997-0.999	0.997	0.994-0.999	0.998	0.996-0.999
Dorsal fontanelle area	0.999	0.998-1.000	0.998	0.995-0.999	0.999	0.997-0.999
Left lateral fontanelle area	0.996	0.970-1.000	0.999	0.988-1.000	0.997	0.987-0.999
Right lateral fontanelle area	0.999	0.989-1.000	1.000	0.996-1.000	0.999	0.995-1.000
Caudal fontanelle area	0.993	0.984-0.997	0.992	0.981-0.996	0.992	0.986-0.995

Note: Intrarater reliability: Fontanelle area intraclass correlation coefficient to assess the repeatability of the measurement of the total, dorsal, left and right lateral, and caudal fontanelle area measurements.
Abbreviations: CI, confidence interval; ICC, intraclass correlation coefficient.

3.3 | Persistent fontanelles in dogs with and without CM/SM-related clinical signs

Of the 50 dogs, 28 (56%) had CM/SM-related clinical signs, and of those, 7 had concurrent diseases (dermatological [2], orthopedic [2], and gastrointestinal [3]) possibly causing clinical signs similar to those of CM and SM. These 7 thus were excluded from the comparison of the number of affected CSs and total fontanelle area in dogs with and without CM/SM-related clinical signs, because these diseases may

cause scratching, pain-related behavior, or gait abnormalities, making it difficult to differentiate the clinical signs from those caused by CM, SM, or CCJ abnormalities. Table 7 describes the clinical signs in the 21 dogs included in the analysis and Table 8 the imaging findings in dogs with and without clinical signs.

The number of CSs affected by PFs was significantly higher ($P \leq .001$) in dogs with CM/SM-related clinical signs (Table 9). Furthermore, the mean ± SD total PF area was significantly larger in dogs with CM/SM-related clinical signs (133.7 ± 214.4; $P = .003$)

when compared to dogs without CM/SM-related clinical signs (33.7 ± 43.3 mm^2). When the mean $\pm$ SD area of the palpable PFs at the (mid-dorsal) top of the skull was compared in dogs with (54.57 ± 60.77 mm^2) and without (28.93 ± 38.70 mm^2) CM/SM-related clinical signs, dogs with CM/SM-related clinical signs had significantly larger fontanelles than those without clinical signs ($P = .03$).

4 | DISCUSSION

Our study shows that PFs are common in adult Chihuahuas. In addition to their well-known location on the dorsal surface of the cranium (ie, the BF), PFs are common at other locations as well. Furthermore, the number of CSs affected by PFs was higher and the PFs larger in dogs with CM/SM-related clinical signs.

4.1 | Persistent fontanelles

The Chihuahuas in our study almost all had either 1 or several PFs emerging on each of their cranial surfaces. The frontoparietal suture (location of the BF) was the CS most commonly affected. In a minority of the dogs, however, the frontoparietal suture was not affected, although the dog had PFs at other CSs. This finding indicates that a BF cannot serve as a marker of these bony lesions elsewhere on the cranial surface.

TABLE 7 Clinical signs observed in the 21 dogs with clinical signs related to Chiari-like malformation or syringomyelia

Clinical sign	Number of dogs (%)
Persistent scratching episodes	16 (76%)
Episodes of facial rubbing	9 (43%)
Spinal hyperesthesia	9 (43%)
Vocalization evoked by scratching, excitement, or movement	9 (43%)
Gait abnormalities: stumbling, incoordination, or weakness	11 (52%)

The BF (a molera) earlier was considered a sign of the purity of the Chihuahua breed. Today, in Chihuahua breed standards of various kennel clubs, the occurrence of a molera as a trait ranges from being accepted to a disqualifying fault, and hence possibly affecting breeding selection.[12-15] The existence of this PF is commonly tested by palpating the head. In adult Chihuahuas, doing so allows recognition only of PFs located in areas of the skull lacking a thick muscle layer (such as the mid-dorsal region). Furthermore, the PFs must be large enough to be recognized by palpation. Because PFs at sites other than that of the BF (midsagittal, dorsal surface of the cranium) are covered by muscle thick enough to hinder palpation, in our experience, palpating only the molera will leave more than half of all PFs undetected.

Only the bregmatic and caudally located fontanelle, resembling the human posterior fontanelle, and here called the occipital fontanelle, is

TABLE 9 Number of cranial sutures affected by persistent fontanelles in dogs with and without clinical signs related to Chiari-like malformation or syringomyelia

Number of cranial sutures affected by persistent fontanelles per dog	Dogs without clinical signs related to CM/SM (%)	Dogs with clinical signs related to CM/SM (%)
0	2 (9%)	1 (5%)
1	14 (64%)	4 (20%)
2	4 (18%)	4 (20%)
3	1 (5%)	3 (15%)
4	1 (5%)	1 (5%)
5	0 (0%)	1 (5%)
6	0 (0%)	3 (15%)
7	0 (0%)	1 (5%)
8	0 (0%)	1 (5%)
9	0 (0%)	0 (0%)
10	0 (0%)	1 (5%)
Total	22	20[a]

Abbreviations: CM, Chiari-like malformation; SM, syringomyelia.
[a]Due to one dog missing computed tomography images of the cranial skull, it was left out from the analysis of total number of cranial sutures affected by persistent fontanelles.

TABLE 8 Diagnostic imaging findings in 43 dogs with and without clinical signs related to Chiari-like malformation or syringomyelia

	Dogs without CM/SM-related clinical signs[a]	Dogs with CM/SM-related clinical signs[a]	Total (%)
CM	22	21	43/43 (100%)
SM	5	12	17/43 (40%)
AOO	16	16	32/43 (74%)
Mean $\pm$ SD medullary kinking index	20% $\pm$ 8%	26% $\pm$ 6%	NA
Mean $\pm$ SD dorsal spinal cord compression index	24% $\pm$ 8%	26% $\pm$ 7%	NA

Abbreviations: AOO, atlanto-occipital overlapping; CM, Chiari-like malformation; NA, not applicable; SM, syringomyelia.
[a]The mean $\pm$ SD age of dogs without CM/SM-related clinical signs was 63 ± 18 months, and in dogs with CM/SM-related clinical signs was 55 ± 36 months.

described in dogs, with the literature lacking any description of the sphenoid and mastoid fontanelles. Based on our results, it appears that the majority of the PF in Chihuahuas occurred in similar locations to fontanelles in humans. In children, however, the fontanelles close during early childhood, the anterior fontanelle between 3 and 27 months.[16,17] The posterior fontanelle is open in only 1.5% of newborn children, and in those it closes by 2 months of age.[18] The paired sphenoid fontanelles close at around 3 month, and the mastoid fontanelles during the second year of life.[8]

4.2 | Inter-rater and intrarater reliabilities of fontanelle area measurement

When assessing both the percentage agreement and Krippendorff's alpha, repeatability of total PF area measurements between the assessors (inter-rater reliability) was almost perfect. Similarly, repeatability of the total PF area within the same assessor (intrarater reliability) reached excellent reliability when both percentage agreement and ICC were assessed. These excellent inter- and intrarater reliabilities suggest that the PF area measurement is repeatable.

4.3 | Persistent fontanelles in dogs with and without CM/SM-related clinical signs

The number of CSs affected by PFs was higher and total PF area larger in dogs with CM/SM-related clinical signs. Furthermore, none of the dogs that were free of CM/SM-related clinical signs had more than 4 CSs affected by PF, and 91% of the dogs had 0 to 2 CSs affected. In dogs with CM/SM-related clinical signs, however, the number of CSs affected by PF ranged from 0 to 10, with only 45% of the dogs having 0 to 2 CSs affected.

As in cavalier King Charles spaniels, SM is an important predisposing factor for CM/SM-related clinical signs in Chihuahuas.[2,19,20] Although SM is an important predisposing factor in dogs that are clinically affected, 1 study (evaluating the association of CM/SM-related clinical signs and morphological traits in Chihuahuas) found that approximately half of the clinically affected Chihuahuas lacked SM.[2] The study found that concomitant occurrence of medullary elevation and dorsal spinal cord compression at C1-2 was associated with a dog's being clinically affected, which implied that CCJ overcrowding itself could predispose to pain-related behavior.[2] Similarly, in cavalier King Charles spaniels, medullary elevation and dorsal spinal cord compression at C1-2 both are associated with CM/SM-related clinical signs.[21,22] Furthermore, a recent study described clinically affected cavalier King Charles spaniels without SM (thought to have CM-related pain) that had an association between short skull base and increased cranial height. This finding indicated more extensive brachycephaly, in addition to ventral olfactory bulb rotation.[23] These findings highlight the importance of cranial-base shortening and resultant compensatory changes in the cranial vault and neural tissue as predisposing factors for development of clinical signs.

Because our clinically affected dogs had both higher numbers of CSs affected by PFs and larger total PF area, we suggest that structures predisposing to CM/SM-related clinical signs may share common pathomechanisms with PF development. The statistical significance and concomitant occurrence, however, does not prove causality between the structures predisposing to clinical signs and PFs. It is unknown why cavalier King Charles spaniels, a breed commonly affected by clinical signs caused by CM or SM, do not empirically appear to have PFs. However, studies evaluating the occurrence of PFs using multimodal imaging techniques in this or other breeds are lacking. Hence, future studies should evaluate if PFs occur in all dogs with structures associated with CM/SM-related clinical signs or if another factor, such as small body (or possibly skull) size, is needed. However, our findings challenge the current notion that PFs are clinically irrelevant findings, especially when occurring in large number and size. Although we find it unlikely that PFs would cause the clinical signs observed in these dogs, we suggest that they share the same pathophysiology with the structures that do cause clinical signs. Based on these findings, critical re-evaluation is necessary for the inclusion of a large BF (molera) in the breed standards as a desired trait. If selection for a "well-rounded 'apple-domed' skull" is made, then PF may be the inevitable consequence for the neuroparenchymal disproportion occurring because of extreme brachycephaly and miniaturization.[14]

4.4 | Possible causes of PFs

Areas deficient in bone can occur as a result of congenital disorders of ossification of developing bone, atrophy of mature bone, or sutural diastasis (delayed closure). Both forms of acquired bone defects, bone remodeling and bone atrophy occur in dogs. In cavalier King Charles spaniels, which like Chihuahuas are also affected by CM, foramen magnum height increases over time, suggesting active supraoccipital bone remodeling due to cerebellar pulsation.[2,24,25] Furthermore, skull bone defects, suggestive of bone atrophy can be a consequence of multiple choroid plexus carcinomas leading to noncommunicating hydrocephalus and increased intracranial pressure.[26]

In children, several conditions cause delayed anterior fontanelle closure, the most common conditions being increased intracranial pressure, congenital hypothyroidism, Down syndrome, rickets, and achondroplasia causing dwarfism.[4] One-third of the PFs in Chihuahuas, however, occurred at locations distinct from the sites of fontanelles described in children, suggesting that in these dogs, skull defect etiology differed. Non-fontanelle anterior bone defects in children may include a lacunar skull or a skull with a diffuse copper-beaten appearance. The first, also called "Lückenshädel skull" (in German, "holes in the skull") is a developmental, congenital failure of bone ossification. The copper-beaten appearance is, in contrast, acquired as a consequence of bone remodeling.[27] Both lesions affect the inner table of the anterior vault, resulting in thinning or loss of bone. The copper-beaten pattern has indistinct margins of varied depth and follows the gyral margins. By contrast, lacunar skull defects have sharply

demarcated margins, are separated by branches of bone, and may appear as full-thickness defects (called craniofenestra).[28-32]

Although both copper-beaten appearance and lacunar skull may occur as incidental findings in children, they are associated with craniosynostosis, a disorder of premature CS closure.[28] Craniosynostosis prevents normal bone growth perpendicular to the affected suture and results in a characteristic head shape typical of that type of craniosynostosis. For example, a bilateral coronal suture synostosis (between the frontal and parietal bones) causes shortening of the skull and results in brachycephaly.[33] Furthermore, it may occur simultaneously with premature cranial base synchondrosis closure causing cranial base shortening.[34]

In brachycephalic dogs, and especially in cavalier King Charles spaniels, the cranial base spheno-occipital synchondrosis closes prematurely, restricting rostrocaudal skull expansion.[35] Furthermore, in Chihuahuas, a short skull base at the caudal cranial fossa and increased proximity of the cervical vertebrae both cause overcrowding of the CCJ which predisposes both to SM and CM/SM-related clinical signs.[2,36] Furthermore, more extreme brachycephaly (ie, a short skull base with compensatory doming of the skull) is associated in cavalier King Charles spaniels with CM-associated pain.[23] Hence, because the CSs affected by PFs are more numerous and the PFs larger in dogs with CM/SM-related clinical signs, and such clinical signs are associated with structures of abnormal cranial shape, a cranial growth disorder such as craniosynostosis may serve as a factor predisposing to PFs.

Based on our study design, and with all but 2 Chihuahuas of our study having been >12 months old, it is impossible to evaluate whether the PFs described here are congenital or acquired defects of bone. Because the present study focuses on describing the distribution and clinical relevance of PFs, future studies should investigate whether PFs are congenital defects of bone ossification, acquired bone remodeling emerging later in life, or result from a combination of these.

4.5 | Limitations of the study

Limitations of our study were related to cohort collection and image analysis. First, most of the Chihuahuas were from the same country, making multicenter studies evaluating international cohorts essential. Furthermore, because participation in the study was voluntary, and hence not randomized, the numbers described here do not necessarily represent the true prevalence of PFs in this breed. Second, evaluation of the PFs occasionally was difficult because of very thin bone and low spatial resolution because of the 2-slice CT imaging equipment's anisotropic data, making it sometimes difficult to differentiate between bone thinning and a true, full-thickness lesion. Because our main aim was to compare findings in dogs with or without CM/SM-related clinical signs, we considered the risk of an error in classification of extremely thin bone as a PF (or the reverse) to be similar in both groups although we did not verify the PFs histologically. Histology was not performed because most of the dogs were alive at the end of the study and thus had not undergone necropsy. Furthermore, because the CSs sometimes were difficult to define, it occasionally was challenging to determine the exact location of the lesion. To overcome these problems, consensus between the evaluators improved the accuracy both of lesion presence and location.

Third, although the PF area measurement method was repeatable, we did not test its validity (ie, its ability to measure the true area of the lesion) because we lacked the necropsy data necessary to compare CT area measurement findings with actual PF areas.

Finally, because no method enabling measurement of these irregular and occasionally very large bone defects located on convex surfaces existed, we developed our own method. One study describes anterior fontanelle area measurement in CT images in children, calculating the surface area by multiplying the width of the fontanelle by its anterioposterior length and dividing that figure by 2.[37] Because of the irregular shape of canine PFs, we were unable to use the same formula. Although studies in dogs describe measurement of the caudal cranial fossa and foramen magnum area using either CT or MRI, we were unable to use either of these methods because of the convexity of the cranial surface (cranial doming) and occasionally large area of the PFs, which made it impossible to delineate some of the PF in a single plane.[19,38-40] Hence, we adopted maximum-intensity projection-technique images to evaluate the extent of the lesions in addition to the number of CSs they affected. This approach allowed us to better compare the findings in dogs with and without CM/SM-related clinical signs. A maximum-intensity projection-technique image is a projection formed from a stack of slices and that projects only the voxel with the highest attenuation value in a 2-dimensional image. This process has been previously described in dogs in angiographic studies to improve mesenteric artery visualization.[41]

To compare findings between dogs with and without CM/SM-related clinical signs, rather than to describe the true area of the lesions, any error in PF area measurement would have affected all dogs in both groups similarly. Our comparison of the total PF area in dogs with and without CM/SM-related clinical signs was similar to comparisons of the number of CSs affected with PFs, but we used a different method (multiplanar reconstruction) of evaluating CT images and used different statistical analyses.

5 | CONCLUSIONS

The lesions described here as PFs were very common in this group of Chihuahuas. The number of PFs varied per dog from single to multiple, and they were located on dorsal, lateral, and caudal surfaces of the cranium. Furthermore, in dogs with CM/SM-related clinical signs, the numbers of CSs affected by PFs were higher and the total PF areas larger in dogs with CM/SM-related clinical signs. Our findings challenge the current notion that PFs, especially when large and occurring multiply, are a clinically irrelevant finding. Furthermore, critical re-evaluation is necessary for the inclusion of a large BF (molera) in the breed standard as a desired trait.

CONFLICT OF INTEREST DECLARATION

Authors declare no conflict of interest.

OFF-LABEL ANTIMICROBIAL DECLARATION

Authors declare no off-label use of antimicrobials.

INSTITUTIONAL ANIMAL CARE AND USE COMMITTEE (IACUC) OR OTHER APPROVAL DECLARATION

The Finnish Animal Experimental Board (ESAVI/5794/04.10.03/2011 and ESAVI/9184/04.10.07/2014) approved obtaining the CT and MR images for diagnostic purposes.

HUMAN ETHICS APPROVAL DECLARATION

Authors declare human ethics approval was not needed for this study.

ORCID

Anna-Mariam Kiviranta https://orcid.org/0000-0002-9542-7247
Clare Rusbridge https://orcid.org/0000-0002-3366-2110
Anu K. Lappalainen https://orcid.org/0000-0002-5675-4771
Jouni J. T. Junnila https://orcid.org/0000-0003-2703-0798
Tarja S. Jokinen https://orcid.org/0000-0001-6389-0109

REFERENCES

1. de Lahunta A, Glass E. Development of the nervous system: malformations. de Lahunta A., Glass E., *Veterinary Neuroanatomy and Clinical Neurology*. 3rd ed. St. Louis, MO: Saunders; 2009:23-53.
2. Kiviranta A-M, Rusbridge C, Laitinen-Vapaavuori O, et al. Syringomyelia and craniocervical junction abnormalities in chihuahuas. *J Vet Intern Med*. 2017;31(6):1771-1781.
3. Evans HE. The fetus. Evans H. E., *Miller's Anatomy of the Dog*. 3rd ed. Philadelphia, PA: Saunders; 1993:48-97.
4. Kiesler J, Ricer R. The abnormal fontanel. *Am Fam Physician*. 2003;67 (12):2547-2552.
5. Opperman LA. Cranial sutures as intramembranous bone growth sites. *Dev Dyn*. 2000;219(4):472-485.
6. Di Ieva A, Bruner E, Davidson J, et al. Cranial sutures: a multidisciplinary review. *Childs Nerv Syst*. 2013;29:893-905. https://doi.org/10.1007/s00381-013-2061-4.
7. Hassan EA, Torad FA, El-Tookhy OS, Shamaa AA. Canine neonatal transcranial ultrasonography from birth until closure of bregmatic fontanelle. *Top Companion Anim Med*. 2015;30(1):5-9.
8. Gray H, Standring S, Ellis H, Berkovitz BKB. *Gray's Anatomy: The Anatomical Basis of Clinical Practice*. 39th ed. Edinburgh, UK: Elsevier Churchill Livingstone; 2006.
9. Hayes AF, Krippendorff K. Answering the call for a standard reliability measure for coding data. *Commun Methods Meas*. 2007;1(1): 77-89.
10. Krippendorff K. Reliability in content analysis: some common misconceptions and recommendations. *Human Commun Res*. 2004;30(3): 411-433.
11. Koo TK, Li MY. A guideline of selecting and reporting intraclass correlation coefficients for reliability research. *J Chiropr Med*. 2016;15: 155-163.
12. American Kennel Club. http://images.akc.org/pdf/breeds/standards/Chihuahua.pdf. Accessed December 20, 2019.
13. Canadian Kennel Club. https://www.ckc.ca/CanadianKennelClub/media/Breed-Standards/Group%205/Chihuahua-Long-Short-Coat.pdf. Accessed December 20, 2019.
14. The Kennel Club. https://www.thekennelclub.org.uk/services/public/breed/standard.aspx?id=6150. Accessed December 20, 2019.
15. Federation Cynologicue Internationale. http://www.fci.be/Nomenclature/Standards/218g09-en.pdf. Accessed December 20, 2019.
16. Duc G, Largo RH. Anterior fontanel: size and closure in term and preterm infants. *Pediatrics*. 1986;78(5):904-908.
17. Boran P, Oğuz F, Furman A, Sakarya S. Evaluation of fontanel size variation and closure time in children followed up from birth to 24 months. *J Neurosurg Pediatr*. 2018;22(3):323-329.
18. Esmaeili M, Esmaeili M, Ghane Sharbaf F, Bokharaie S. Fontanel size from birth to 24 months of age in Iranian children. *Iran J Child Neurol*. 2015;9(4):15-23.
19. Cerda-Gonzalez S, Olby NJ, McCullough S, et al. Morphology of the caudal fossa in Cavalier King Charles Spaniels. *Vet Radiol Ultrasound*. 2009;50(1):37-46.
20. Rusbridge C, Carruthers H, Dubé MP, Holmes M, Jeffery ND. Syringomyelia in Cavalier King Charles Spaniels: the relationship between syrinx dimensions and pain. *J Small Anim Pract*. 2007;48: 432-436.
21. Cerda-Gonzalez S, Olby NJ, Griffith EH. Medullary position at the craniocervical junction in mature Cavalier King Charles Spaniels: relationship with neurologic signs and syringomyelia. *J Vet Intern Med*. 2015;29:882-886.
22. Cerda-Gonzalez S, Olby NJ, Griffith EH. Dorsal compressive atlantoaxial bands and the craniocervical junction syndrome: association with clinical signs and syringomyelia in mature Cavalier King Charles Spaniels. *J Vet Intern Med*. 2015;29:887-892.
23. Knowler SP, Cross C, Griffiths S, et al. Use of morphometric mapping to characterise symptomatic Chiari-like malformation, secondary syringomyelia and associated brachycephaly in the Cavalier King Charles Spaniel. *PLoS One*. 2017;12(1):e0170315. https://doi.org/10.1371/journal.pone.0170315.
24. Driver CJ, Watts V, Bunck AC, Van Ham LM, Volk HA. Assessment of cerebellar pulsation in dogs with and without Chiari-like malformation and syringomyelia using cardiac-gated cine magnetic resonance imaging. *Vet J*. 2013;198(1):88-91.
25. Driver CJ, De Risio L, Hamilton S, et al. Changes over time in craniocerebral morphology and syringomyelia in Cavalier King Charles spaniels with Chiari-like malformation. *BMC Vet Res*. 2012;8:215.
26. Hughes JR, Taylor-Brown FE, Greville-Heygate O, Constantino-Casas F, Williams DL, Genain M. Multimodality characteristics of multifocal choroid plexus carcinoma with bilateral calvarial defects in a dog. *Vet Radiol Ultrasound*. 2019;1–6. https://doi.org/10.1111/vru.12732.
27. Choudhri AF. Skull and scalp. Lamsback W. *Pediatric Neuroradiology: Clinical Practice Essentials*. New York, NY: Thieme; 2017:126-134.
28. Tuite GF, Evanson J, Chong WK, et al. The beaten copper cranium: a correlation between intracranial pressure, cranial radiographs, and computed tomographic scans in children with craniosynostosis. *Neurosurgery*. 1996;39(4):691-699.
29. Leeuwen KV. Lacunar skull of the newborn infant. *J Pediatr*. 1946;28 (2):193-199.
30. Agrawal D, Steinbok P, Cochrane DD. Significance of beaten copper appearance on skull radiographs in children with isolated sagittal synostosis. *Childs Nerv Syst*. 2007;23(12):1467-1470.

31. Poonia A, Giridhara P, Sheoran D. Copper beaten skull. *J Pediatr*. 2019;206:297.

32. Bourekas EC, Lanzieri CF. The calvarium. *Semin Ultrasound CT MR*. 1994;15(6):424-453.

33. Governale LS. Craniosynostosis. *Pediatr Neurol*. 2015;53(5):394-401.

34. Coll G, Sakka L, Botella C, et al. Pattern of closure of skull base synchondroses in Crouzon syndrome. *World Neurosurg*. 2018;109:e460-e467.

35. Schmidt MJ, Volk H, Klingler M, Failing K, Kramer M, Ondreka N. Comparison of closure times for cranial base synchondroses in mesaticephalic, brachycephalic, and Cavalier King Charles Spaniel dogs. *Vet Radiol Ultrasound*. 2013;54(5):497-503.

36. Knowler SP, Kiviranta AM, McFadyen AK, Jokinen TS, La Ragione RM, Rusbridge C. Craniometric analysis of the hindbrain and craniocervical junction of chihuahua, affenpinscher and Cavalier King Charles Spaniel dogs with and without syringomyelia secondary to Chiari-like malformation. *PLoS One*. 2017;12(1):e0169898. https://doi.org/10.1371/journal.pone.0169898.

37. Pindrik J, Ye X, Ji BG, Pendleton C, Ahn ES. Anterior fontanelle closure and size in full-term children based on head computed tomography. *Clin Pediatr*. 2014;53(12):1149-1157.

38. García-Real I, Kass PH, Sturges BK, Wisner ER. Morphometric analysis of the cranial cavity and caudal cranial fossa in the dog: a computerized tomographic study. *Vet Radiol Ultrasound*. 2004;45(1):38-45.

39. Couturier J, Rault D, Cauzinille L. Chiari-like malformation and syringomyelia in normal cavalier King Charles spaniels: a multiple diagnostic imaging approach. *J Small Anim Pract*. 2008;49(9):438-443.

40. Carrera I, Dennis R, Mellor DJ, Penderis J, Sullivan M. Use of magnetic resonance imaging for morphometric analysis of the caudal cranial fossa in Cavalier King Charles Spaniels. *Am J Vet Res*. 2009;70(3):340-345.

41. Lee S-K, Yoon S, Kim C, Choi J. Triple-phased mesenteric CT angiography using a test bolus technique for evaluation of the mesenteric vasculature and small intestinal wall contrast enhancement in dogs. *Vet Radiol Ultrasound*. 2019;60:493-501.